



RESEARCH ARTICLE

10.1002/2015EA000113

Key Points:

- UAVSAR and GPS results of the M5.1 La Habra earthquake show broad deformation
- Concurrent slip on several shallow structures best explains the observations
- We show a time-independent means of estimating the potential for future events

Correspondence to:

A. Donnellan,
andrea.donnellan@jpl.nasa.gov

Citation:

Donnellan, A., L. Grant Ludwig, J. W. Parker, J. B. Rundle, J. Wang, M. Pierce, G. Blewitt, and S. Hensley (2015), Potential for a large earthquake near Los Angeles inferred from the 2014 La Habra earthquake, *Earth and Space Science*, 2, doi:10.1002/2015EA000113.

Received 14 APR 2015

Accepted 15 AUG 2015

Accepted article online 19 AUG 2015

Corrected 07 OCT 2015

This article was corrected on 07 OCT 2015.
See the end of the full text for details.

©2015. The Authors.

This is an open access article under the terms of the Creative Commons Attribution-NonCommercial-NoDerivs License, which permits use and distribution in any medium, provided the original work is properly cited, the use is non-commercial and no modifications or adaptations are made.

Potential for a large earthquake near Los Angeles inferred from the 2014 La Habra earthquake

Andrea Donnellan^{1,2}, Lisa Grant Ludwig³, Jay W. Parker¹, John B. Rundle⁴, Jun Wang⁵, Marlon Pierce⁵, Geoffrey Blewitt⁶, and Scott Hensley¹

¹Jet Propulsion Laboratory, California Institute of Technology, Pasadena, California, USA, ²Department of Earth Sciences, University of Southern California, Los Angeles, California, USA, ³Program in Public Health, University of California, Irvine, California, USA, ⁴Departments of Physics and Geology, University of California, Davis, California, USA, ⁵University Information Technology Services, Indiana University, Bloomington, Indiana, USA, ⁶Nevada Geodetic Laboratory, Nevada Bureau of Mines and Geology, University of Nevada, Reno, Nevada

Abstract Tectonic motion across the Los Angeles region is distributed across an intricate network of strike-slip and thrust faults that will be released in destructive earthquakes similar to or larger than the 1933 *M*_{6.4} Long Beach and 1994 *M*_{6.7} Northridge events. Here we show that Los Angeles regional thrust, strike-slip, and oblique faults are connected and move concurrently with measurable surface deformation, even in moderate magnitude earthquakes, as part of a fault system that accommodates north-south shortening and westerly tectonic escape of northern Los Angeles. The 28 March 2014 *M*_{5.1} La Habra earthquake occurred on a northeast striking, northwest dipping left-lateral oblique thrust fault northeast of Los Angeles. We present crustal deformation observation spanning the earthquake showing that concurrent deformation occurred on several structures in the shallow crust. The seismic moment of the earthquake is 82% of the total geodetic moment released. Slip within the unconsolidated upper sedimentary layer may reflect shallow release of accumulated strain on still-locked deeper structures. A future *M*_{6.1–6.3} earthquake would account for the accumulated strain. Such an event could occur on any one or several of these faults, which may not have been identified by geologic surface mapping.

1. The 2014 *M*_{5.1} La Habra Earthquake

The *M*_{5.1} La Habra earthquake occurred on 28 March 2014 at a depth of ~5.85 km (33.9225°N, 117.9352°W) beneath suburban La Habra at the northeastern margin of the Los Angeles basin [Wright, 1991] in southern California. Global Positioning System (GPS) geodesy and interferometric synthetic aperture radar (InSAR) show that the northern Los Angeles region is shortening at a rate of 4.5 ± 1 mm/yr in a north-south direction [Argus *et al.*, 2005]. The style of tectonic deformation in the region is influenced by northwest trending right-lateral strike-slip faults associated with the Peninsular Ranges and San Andreas plate boundary fault system, and north-south shortening along north dipping thrust faults, often associated with oblique left-lateral motion and east-west trending folds of the Transverse Ranges [Yeats, 2004]. Seismic hazard assessments for the region have focused on major faults such as the strike-slip Newport-Inglewood fault that caused the destructive 1933 *M*_w 6.4 Long Beach earthquake [Hauksson and Gross, 1991] and the blind thrust system that generated the 1994 *M*_{6.7} Northridge earthquake [Walls *et al.*, 1998].

The La Habra earthquake sequence occurred between the right-lateral strike-slip Whittier fault and the Puente Hills thrust fault, above a regional decollement [Yang and Hauksson, 2011]. A surprising amount of damage occurred, despite the moderate main shock magnitude and peak ground accelerations of 0.7 g and 0.35 g northeast and southeast of and near the epicenter (USGS: Peak ground acceleration for La Habra earthquake, <http://earthquake.usgs.gov/earthquakes/shakemap/sc/shake/15481673/stationlist.html#sCE.13883>). More than a dozen water mains broke in La Habra and Fullerton alone [Tully and Casiano, 2014], and widespread damage to infrastructure in Orange County exceeded \$12 M [Wiskol, 2014]. We documented 13 water main breaks, a gas line break, and numerous pavement cracks associated with the earthquake sequence. Most of these were within a 6 km radius of the epicenter and mostly occurred outside of the earthquake zone of seismicity with about half of the water main breaks occurring in the West Coyote Hills to the south (Figure 1).

The 5.85 km deep main shock was followed by a relatively shallow aftershock sequence extending upward from a depth of 7 km to approximately 3 km below the communities of La Habra, Fullerton, and Brea. The

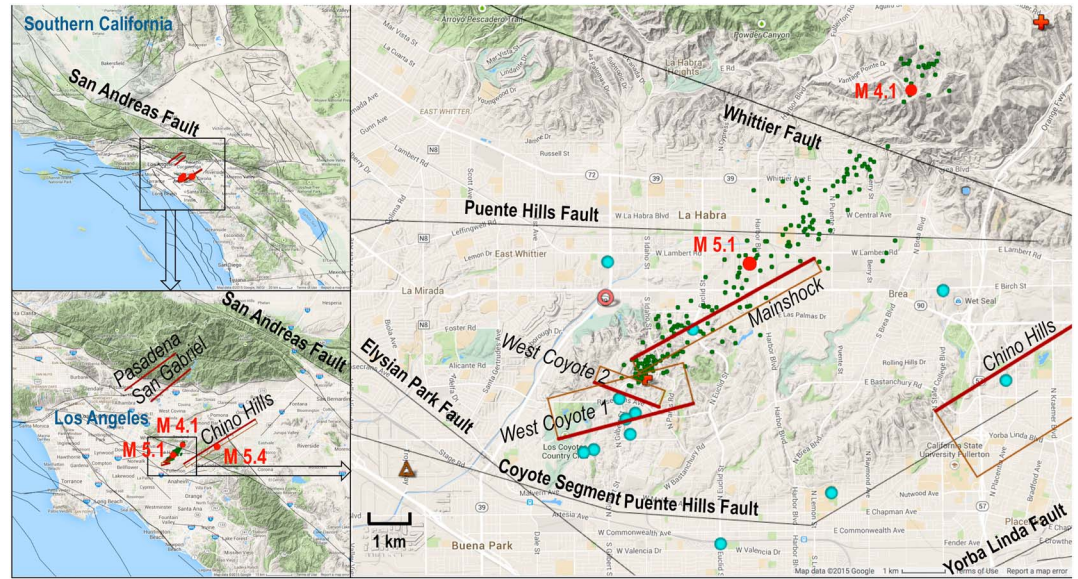


Figure 1. Setting of the La Habra earthquake. Red dots show locations of the M5.1 main shock, M4.1 aftershock, and M5.4 Chino earthquake. Relocated aftershocks are shown as green dots. Modeled faults are shown in brown with the heavier reddish brown line denoting the bottom of the fault and labeled with italics. Water main breaks are shown as blue dots, a gas line break as a red open circle, an observed fault kink band near Trojan Way as a triangle, and road cracks as red crosses. Faults from the UCERF-3 models [Field et al., 2013] are shown as dark grey lines.

northeast trend of aftershocks is consistent with one of the focal mechanism solutions, indicating main shock rupture of a northeast striking, northwest dipping left-lateral oblique thrust fault. The largest aftershock, M4.1, occurred on 29 March 2014 at a depth of 6.38 km (33.9563°N, 117.8970°W). Both events were widely felt in Southern California, with residents reporting maximum main shock instrumental intensity of VII in the La Habra and Brea epicentral area. The relatively strong shaking and large-area extent of reported motion are consistent with the shallow depth of the sequence.

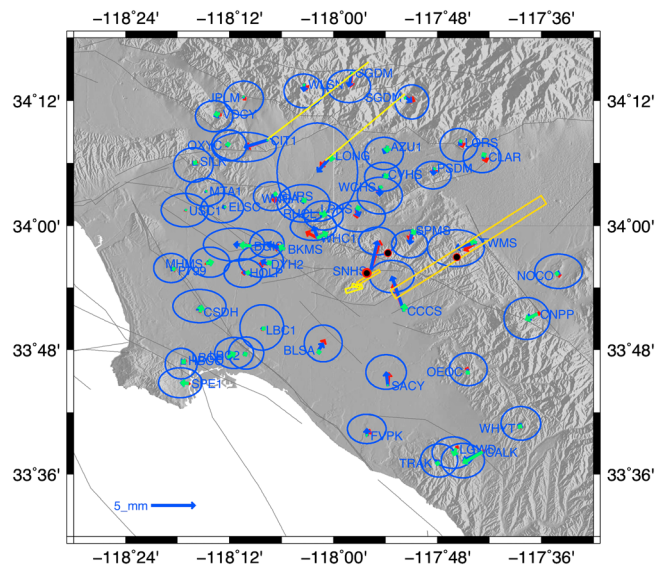


Figure 2. Displacements at the time of the La Habra earthquake for GPS stations within a 50 km radius of the epicenter (red circle around black dot near SNHS). The error ellipses around the blue observed GPS vectors represent 95% confidence. Red arrows are the calculated vectors and green the model residuals. Modeled faults are shown. The M5.1 main shock, M4.1 aftershock, and M5.4 Chino Hills earthquake are noted by red circles around a black dot.

2. Geodetic Measurements Indicate a Broad Pattern of Crustal Deformation

We determined displacements that occurred as a result of the 28 March 2014 M5.1 La Habra earthquake using GPS and Uninhabited Aerial Vehicle Synthetic Aperture Radar (UAVSAR) measurements. Both the GPS and UAVSAR measurements show a broader pattern of deformation than would be expected from a M5.1 earthquake.

We used daily GPS positions produced by the University of Nevada, Reno, within a 50 km radius of the La Habra earthquake to estimate offsets from the event [Blewitt et al., 2013]. We averaged daily positions for these 32 stations for 15 days before the event and differenced those from 14 day averages after

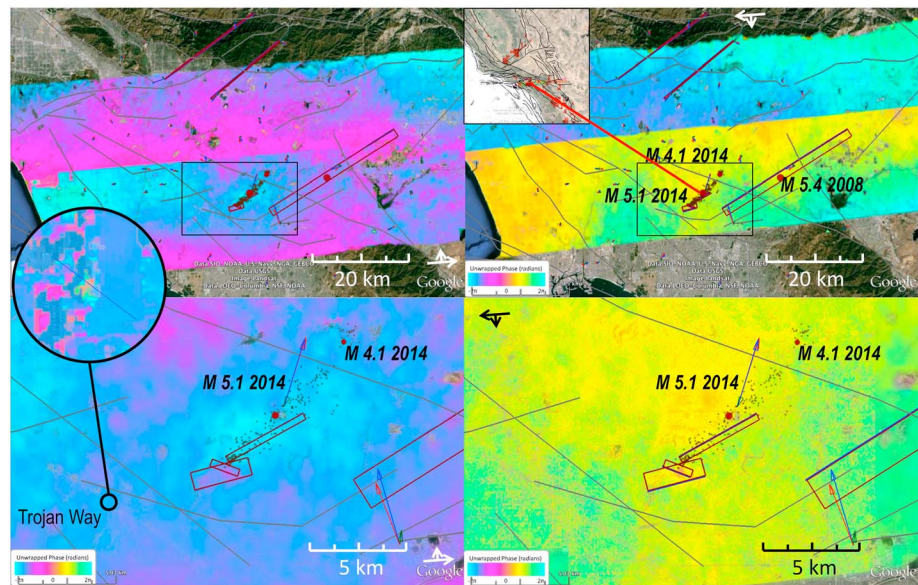


Figure 3. UAVSAR observations spanning the La Habra earthquake. The inset location map shows Southern California with the 2007 forecast for likely earthquakes shown as red areas. (top left) Northward looking lines with 08521 covering La Habra to the south and 08523 covering the San Gabriel Valley to the north. (top right) The southward looking lines with 26522 covering La Habra and 26524 covering the San Gabriel Valley. (bottom) The region around La Habra. The circle shows the detail of the Trojan Way kink band observed with UAVSAR. The discontinuity across the tracks is due to the ground elevation or look angle varying by 40° across the swath due to the aircraft flying at a much lower elevation than a spacecraft. The overlapping swaths cannot be matched without making assumptions about ground deformation.

the event. The GPS results (Figure 2) show a pattern of north-south shortening and westward motion aligned with the center of the zone of convergence, which extends about 35 km north and 20 km south of the La Habra earthquake epicenter. The band of westward extrusion is about 40 km wide, extending 25 km west and 15 km east of the epicenter.

Since 2009, we have collected measurements from NASA's UAVSAR L band radar instrument to monitor deformation across the Los Angeles region. The Los Angeles region was selected in part to test earthquake forecasting methodology [Rundle *et al.*, 2002, 2003; Tiampo *et al.*, 2002; Holliday *et al.*, 2005, 2007], which indicated a high probability of a $> M5.0$ earthquake at the front of the Transverse Ranges in the Chino Hills area. North and south looking UAVSAR lines were flown before the earthquake on 22 January 2014. The north looking line was remeasured 3 days after the earthquake on 31 March 2014, and the south looking line was remeasured a week after the event on 4 April 2014. The UAVSAR Repeat Pass Interferometry (RPI) products show uplift that is consistent with the location of the main shock beneath the town of La Habra (Figure 3). The results also show considerable aseismic northward horizontal deformation with minor uplift in the West Coyote Hills, south of the relocated seismicity. A small narrow band of shortening was also observed with UAVSAR, and confirmed with on the ground field observations, at the Trojan Way Kink Band, nearly one fault dimension southwest of the main rupture.

UAVSAR data can have large errors on the scale of several km from unmodeled aircraft motion and troposphere error, but it is very precise over a few hundred meters. Both error sources are of a short duration. The results of the image pairs we show here were for lines flown with opposite looks hours apart on 22 January 2014, and 4 days apart following the earthquake and troposphere errors would not be correlated. The results near the epicenter are consistent with spaceborne InSAR images of the event [Fielding *et al.*, 2015]. The UAVSAR measurements were optimally oriented to detect the northward motion of the West Coyote Hills and shortening of the Trojan Way kink band. The northerly tracks of the spaceborne radar assets were subparallel to the direction of motion of those two features and as a result were not sensitive to motion in the northerly direction.

3. Several Structures Produce the Observed Deformation

Movement on several active geological structures is necessary to produce the observed ground deformation. We inverted the GPS and UAVSAR measurements with numerous starting nominal fault parameters to determine the

Table 1. Modeled Structures and Slip That Produce the Observed Deformation Field Based on Inversions of GPS and UAVSAR Observations^a

	Main Shock	West Coyote 1	West Coyote 2	Chino	San Gabriel	Pasadena
Latitude (start/end)	33.92351°/33.90384°	33.88804°/33.89497°	33.89949°/33.89444°	34.04059°/33.89283°	34.20739°/34.09973°	34.13619°/34.25911°
Longitude (start/end)	-117.91991°/-117.96282°	-117.98022°/-117.94822°	-117.97217°/-117.95660°	-117.60800°/-117.89272°	-117.86546°/-118.02372°	-118.12688°/-117.92404°
Strike (left lateral)	-119°	75°	111°	-122°	-129°	54°
Dip	70° (NW)	4° (SE)	15° (SW)	66° (NW)	55° (NW)	73° (SE)
Depth (bottom/top)	4.6 km/3.7 km	0.2 km/0.1 km	0.2 km/0.1 km	4.0 km/0.1 km	0.7 km/0.4 km	0.2 km/0.0 km
Width	1.0 km	0.9 km	0.4 km	4.3 km	0.4 km	0.2 km
Length	4.5 km	3.1 km	1.5 km	31.0 km	18.9 km	23 km
Strike slip	353 mm	0.3 mm	-39 mm	4 mm	12 mm	12 mm
Dip slip (thrust)	490 mm	31 mm	49 mm	3 mm	33 mm	4 mm
Rigidity (dyne/cm ²)	2.0×10^{11}	8.6×10^9	8.4×10^9	8.2×10^{10}	2.7×10^{11}	2.2×10^{10}
Moment (dyne · cm)	5.48×10^{22}	7.42×10^{20}	3.17×10^{20}	5.48×10^{22}	7.07×10^{22}	1.26×10^{24}
M_w	5.1	3.2	3.0	4.5	4.5	3.4

^aThe faults in the table represent the general characteristics of the structures responsible for the deformation. Total summed moment of all the modeled segments is 6.76×10^{23} dyne · cm.

structures responsible for the observed deformation field. We use the χ^2/dof to determine the goodness of fit. The χ^2/dof for the final model here is 1.3. Our best fit model was built up by inverting for deformation on individual structures in subregions identified by surface deformation gradients in the GPS or UAVSAR data. Because all of the modeled structures are buried, we cannot identify them in the field. The data are best fit by the following deformation sources, with parameters shown in Table 1. Left-lateral oblique thrust motion is associated with the main shock and bounds the southeast margin of the aftershock zone. Movement occurred on shallow low-angle northward thrusts in the West Coyote Hills and on a fairly extensive but low-slip northeast striking northwest dipping oblique left-lateral fault crossing the Chino Hills (Figures 1–3 and Table 1). Shallow deformation also occurred in the San Gabriel Valley and can best be explained by a pair of northeast striking left-lateral shear zones. Shallow low-angle motion of the upper sediments can also explain the motion, but that solution is not as robust. The suite of faults is located within an intricate structural zone where deformation from regional strike-slip and thrust systems overlaps. The modeled faults represent the general characteristics of the active structures, with the styles and locations noted emerging in the majority of the inversions.

The location of the earthquake main shock and aftershock zone is northwest of but subparallel to the Coyote Hills segment of Puente Hills thrust fault [Shaw *et al.*, 2002; Pratt *et al.*, 2002]. The location, orientation, and mechanism of the modeled main shock fault (Table 1) are coincident with the approximate location of a “tear fault” in the Coyote Hills (CH) segment of the Puente Hills fault inferred by Shaw *et al.* [2002] connecting thrust ramps beneath the West and East Coyote Hills oil fields.

Modeling reveals the presence of gently dipping shallow planes in the West Coyote Hills, West Coyote 1, and West Coyote 2 (Table 1), which caused northward horizontal deformation of the hills. The deformation can be seen in the interferograms as color gradients associated with the West Coyote Hills modeled structures (Figures 3 and 4). Combining the north and south looks enables estimation of horizontal and vertical motions (Figure 4). The combined looks indicate about 80 mm of northward horizontal motion with a slight amount of uplift totaling 5–10 mm. The dips in the points along the horizontal profile at about 0.3, 0.7, and 1.1 km correlate with roads, suggesting that the roads restrained the northward motion at the surface. The shallow depth of our modeled faults, West Coyote 1 and West Coyote 2, suggests that they are associated with a prominent shallow dipping structure identified on seismic reflection images by Pratt *et al.* [2002] as possibly an unconformity at 0.2–1.0 km depth, or they are consistent with the bedding planes indicated on the map in Figure 3 of Pratt *et al.* [2002]. These structures are linked with fold growth and movement of the deeper Puente Hills thrust.

4. Shallow Deformation Reflects Strain Accumulation on Deeper Faults

There is controversy about whether a blind thrust fault, such as the Puente Hills thrust, or a strike-slip fault poses greater hazard to the metropolitan region. Limitations of the data and models preclude us from

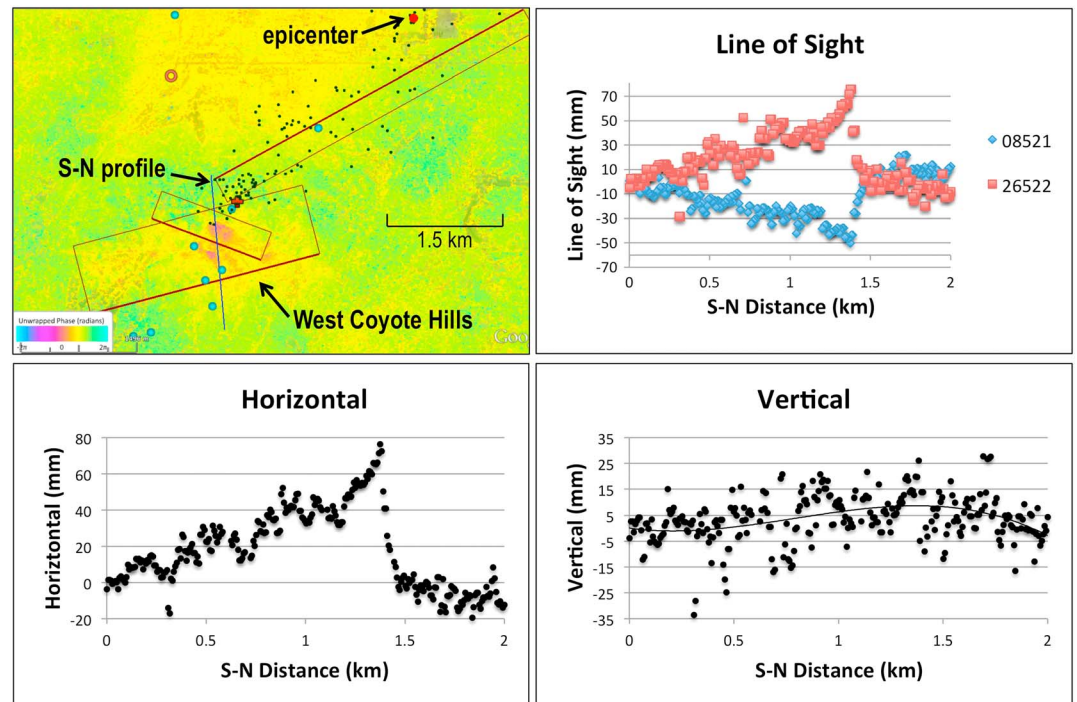


Figure 4. West Coyote Hills UAVSAR observation for south looking line 26522. (top left) A blue line marks the south to north profile shown in the plots. (top right) The line of sight observations show opposite change in range between the ground and the instrument. The two looks were combined to produce estimates of (bottom left) horizontal and (bottom right) vertical motion. A trend line is fit through the plot of vertical motion.

accurately determining this; however, *Myers et al.* [2003] estimate a long-term slip rate of 1.3 mm/yr on this section of the Puente Hills thrust. Approximately 32 mm of displacement should have accumulated since the 1989 Whittier Narrows earthquake, which is roughly consistent with the shallow slip that we estimated. The overlying sediments that are less compliant than deeper sediments may have relieved accumulated strain that is still present on the Puente Hills thrust.

Shallow seismic reflection profiles along Trojan Way in the west Coyote Hills [*Pratt et al.*, 2002; *Shaw et al.*, 2002; *Leon et al.*, 2007] reveal active folding related to movement of the Puente Hills blind thrust. A 9 m high surface scarp across Trojan Way has been interpreted as the surface expression of an active synclinal axial surface, or kink band, consistent with uplift and folding on the underlying Coyote Hills segment of the Puente Hills thrust [*Pratt et al.*, 2002]. This kink band is 9 km southwest of the main shock epicenter but shows activation in the UAVSAR repeat pass interferometry in the 22 January to 31 March 2014 pair. Our postseismic field investigation identified a zone of cracks that correlates with UAVSAR fringes, which show 4 cm of ground range change of the ground toward the instrument. About 10 km farther west, a narrow <145 m anticline has been identified in the geologic data as an upward termination of the Puente Hills blind thrust fault [*Dolan et al.*, 2003]. The orientation of our measured deformation trends more northeasterly than this east-northeast structure but is consistent with the arcuate expression of the faults and other structures.

The modeled northeast striking shear zones in the San Gabriel Valley and Chino Hills (Figure 2 and Table 1) are part of a series of incompletely mapped active left-lateral oblique faults in a structurally complex zone. The modeled faults extend northeast from mapped segments of the Raymond, Elysian Park, and Puente Hills faults. Recent moderate magnitude left-lateral strike-slip mechanism earthquakes on this system include the 2008 M_w 5.4 Chino Hills earthquake (33.95°N, 117.76°W), which is coincident with the modeled Chino Hills structure, the 1988 M_w 4.9 Pasadena earthquake on the Raymond fault, the 1988 and 1990 M_L 4.6 and M_L 5.2 Upland earthquakes on the buried San Jose fault, and the 1991 M 5.6 Sierra Madre earthquake on the Clamshell-Sawpit fault. Notable northeast striking alignments of seismicity include the Yorba Linda [*Yeats*, 2004] and the Fontana [*Hauksson and Jones*, 1991] seismicity trends, which are subparallel to the San Gabriel and Chino shear zones revealed by our inversion of UAVSAR and GPS data. The Fontana

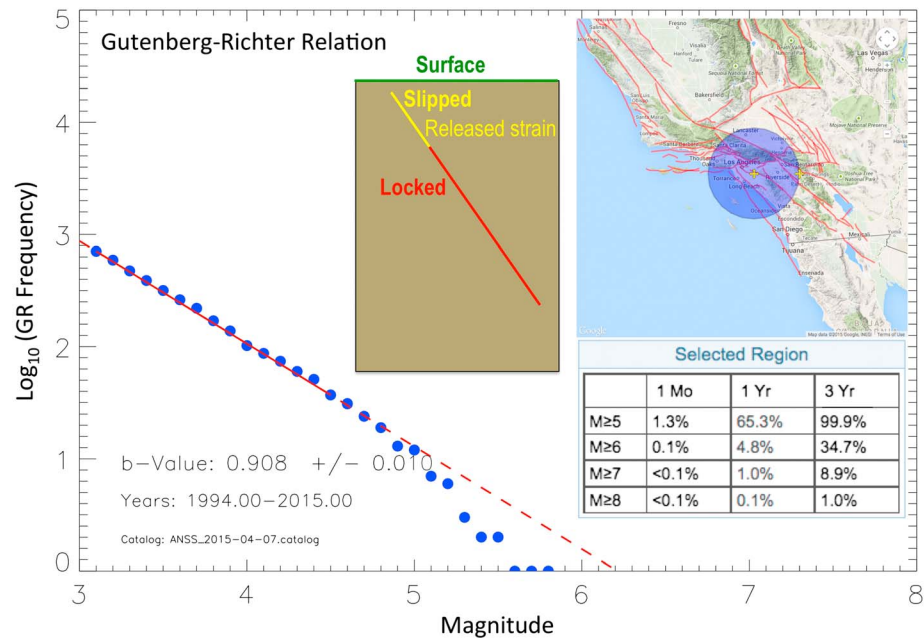


Figure 5. Gutenberg-Richter relation for a 100 km radius circle from the La Habra earthquake epicenter since the 1994 $M_{6.7}$ Northridge earthquake. Top right inset shows the region of interest. Table shows the probably of occurrence of events of different magnitude of different time frames. Seismicity data are from the Advanced National Seismic System (2015, <http://www.quake.geo.berkeley.edu/anss/catalog-search.html>) and U.S. Geological Survey (2015, http://earthquake.usgs.gov/earthquakes/states/events/1952_07_21.php). Inset shows a cross section illustrating the concept of slip in the upper sediments releasing shallow accumulated strain while the lower fault segment remains locked.

seismicity trend aligns with the epicenter of the 2008 Chino Hills earthquake and projects southwestward into the Coyote Hills segment of the Puente Hills thrust. The modeled fault connects the seismicity trend and the Puente Hills thrust.

Our results are consistent with north-south shortening and westward escape of the crust near Los Angeles. The La Habra earthquake that occurred at the northeastern margin of the Los Angeles Basin reflects a broader pattern of north-south shortening and westward escape of the upper crust [Walls *et al.*, 1998]. This area marks the transition between two tectonic regimes where regional right-lateral shear is accommodated by major northwest trending faults of the Peninsular Ranges, and north-south shortening is accommodated by north dipping thrust faults and east-west trending folds of the Transverse Ranges (Hauksson and Jones, 1991; Seeber and Armbruster, 1995; Yeats, 2004; Yang and Hauksson, 2011).

5. Deeper Locked Faults Have the Potential to Produce a Large Earthquake

The 2014 $M_{5.1}$ La Habra earthquake was a small reflection of a larger episode of deformation that occurred concurrently with the earthquake. We used the modeled fault parameters (Table 1) and the Southern California Earthquake Center (SCEC) Velocity 4 model to calculate the rigidity from V_s and density at the center of each modeled structure [Kohler *et al.*, 2003] to estimate the geodetic moment, which is the area of the fault multiplied by slip on the fault and rigidity [Kanamori, 1978]. The seismic moment of this $M_{5.1}$ earthquake is 5.52×10^{11} dyne/cm², which is 82% of the total observed geodetic moment of 6.76×10^{23} dyne·cm. The geodetic and seismic moment of the mainshock ruptures match, but the total geodetic moment is equivalent to an $M_{5.2}$ earthquake. The earthquake main shock accounts for 100% of the geodetic moment estimated for the main shock fault alone. 18% of the deformation occurred regionally and aseismically.

The observed ground deformation could represent release of accumulated tectonic strain or be the result of dynamic shaking along weaker structures than the surrounding area. If it is related to release of accumulated strain, then it provides an estimate for the amount of strain accumulated at depth that has not yet been released. Using the observed slip and modeled structures as a guide, we estimate the potential for a future

earthquake if these structures were to rupture from the base of the seismogenic zone to the base of the modeled faults (Figure 5, inset). The results for a potential earthquake range from $M6.1$ for a seismic moment release of 82% of the total release and a seismogenic depth of 15 km to a $M6.3$ event for 100% of the release occurring seismically and a 20 km depth of the base of the seismogenic zone. Paleoearthquake evidence suggests the Puente Hills blind thrust has produced earthquakes in the M_w 7.2–7.5 range in the last 11,000 years [Dolan *et al.*, 2003]. Using seismic data, Sleep [2015] and Roten *et al.* [2014] reach similar conclusions that the upper compliant sediments relieve accumulated strain during moderate to large earthquakes: The uppermost few hundred meters of rock fails in oscillating dynamic friction beneath Whittier Narrows [Roten *et al.*, 2014], and the ambient fault-normal stress relaxes during the process over time accommodating the shallow tectonic strain [Sleep, 2015]. Repeated strong shaking keeps the shallow ambient stress at low levels. Mori and Abercrombie [1997] find that deeper earthquakes are more likely to grow into large earthquakes, which also suggests that strain is relieved aseismically or more regularly in the upper crust.

The Gutenberg-Richter relation for a 100 km radius circle around the La Habra earthquake epicenter for events beginning just after the 1994 $M6.7$ Northridge earthquake shows a deficiency of earthquakes $M > 5$ (Figure 5), which is consistent with our analysis of the geodetic data. The deficit of earthquakes having $\sim M5$ and larger can be seen relative to the scaling line. The B value shown here is consistent with B values for Southern California determined by Mori and Abercrombie [1997] for earthquakes > 9 km depth. For the Gutenberg-Richter relation to be completed, this deficit must eventually be filled with large earthquakes, up to $M6.2$, which is consistent with the above analysis. We assign a probability to these large earthquakes using a Weibull distribution [Weibull, 1951] and the assumption that over long times and large regions the Gutenberg-Richter magnitude-frequency relation is linear [Rundle *et al.*, 2012; Holliday *et al.*, 2014; Rundle *et al.*, 2016]. The calculated probability for a $M \geq 6$ earthquake within a circle of radius 100 km, and over the 3 years following 1 April 2015, is 35%. For a $M \geq 5$ earthquake within a circle of radius 100 km, and over the 3 years following 1 April 2015, the probability is 99.9%.

Our results indicate that significant ground deformation and infrastructure damage can occur beyond the epicentral region of a moderate earthquake near Los Angeles. Identifying specific structures most likely to be responsible for future earthquakes is difficult for this intricate network of active faults and presence of weak slip planes. The observed widespread and largely aseismic slip may be because the Puente Hills thrust and related faults are structurally immature [Dolan and Haravitch, 2014]. Geodetic imaging of active structures, however, can be used to identify the full extent of slip and provide a time-independent means of estimating a lower bound of future earthquake potential. In the La Habra and Puente Hills area observed here, the lower bound for a potential earthquake is $M6.1$ – 6.3 .

Author Contributions

This text was written primarily by Andrea Donnellan and Lisa Grant Ludwig. Andrea Donnellan, Scott Hensley, John Rundle, and Jay Parker conceived the UAVSAR experiment over the Los Angeles area. Andrea Donnellan led the modeling and interpretation of the UAVSAR and GPS data. Lisa Grant Ludwig led the geological interpretation and participated in the fieldwork with Andrea Donnellan. Scott Hensley leads the UAVSAR project including development of the instrument and processing of the data. Geoffrey Blewitt provided the processed daily GPS solutions. Jay Parker estimated the GPS offsets of the earthquake and developed software tools for inverting the GPS and UAVSAR observations. Marlon Pierce and Jun Wang led the development of the computational infrastructure for analyzing, inverting, and visualizing the results presented in this paper. Andrea Donnellan led the estimation of earthquake potential based on the geodetic inversion results. John Rundle led the estimate of earthquake potential and probability based on the seismic data.

References

- Argus, D. F., M. B. Heflin, G. Peltzer, F. Crampe, and F. H. Webb (2005), Interseismic strain accumulation and anthropogenic motion in metropolitan Los Angeles, *J. Geophys. Res.*, *110*, B04401, doi:10.1029/2003JB002934.
- Blewitt, G., C. Kreemer, W. C. Hammond, and J. M. Goldfarb (2013), Terrestrial reference frame NA12 for crustal deformation studies in North America, *J. Geodyn.*, *72*, 11–24, doi:10.1016/j.jog.2013.08.004.
- Dolan, J. F., and B. D. Haravitch (2014), How well do surface slip measurements track slip at depth in large strike-slip earthquake? The importance of structural maturity in controlling on-fault slip versus off-fault surface deformation, *Earth Planet. Sci. Lett.*, *388*, 38–47, doi:10.1016/j.epsl.2013.11.043.

Acknowledgments

This work was carried out at the Jet Propulsion Laboratory, California Institute of Technology under contract with NASA. The work was funded by NASA's EarthScope Geodetic Imaging UAVSAR program, Advanced Information Systems Technology (AIST) program for QuakeSim work, and the ACCESS program for GeoGateway development. We thank the city of Fullerton personnel for information on water main breaks. Margaret Glasscoe, Erik Conway, and John Casani assisted with the fieldwork to validate the UAVSAR observations. We thank Egill Hauksson for the relocated earthquakes, discussion, and his thoughtful reviews of this paper. We also thank James Dolan for his discussion and interest in this work. We thank the UAVSAR team and in particular Yunling Lou, Brian Hawkins, Naiara Pinto, and Yang Zheng for collection and processing of the UAVSAR data. The GPS analysis was funded by NASA grants NNX14AJ52A, NNX12AK26G, and NSF grant EAR-1252210. GPS data were processed using the GIPSY OASIS II software and data products from JPL, with ocean loading coefficients by Hans-Georg Scherneck. We are grateful for data provided by the International GNSS Service and the EarthScope Plate Boundary Observatory operated by UNAVCO Inc. We used <http://geo-gateway.org> for analysis of the data, which can be used for modeling and accessing UAVSAR data products from the Alaska Satellite Facility. GPS data products can be accessed from <http://geodesy.unr.edu>. We particularly thank two reviewers for *Earth and Space Science* and Donald Argus whose careful reads and comments improved this paper. We thank Rob Graves of the USGS Pasadena for input on our seismic moment calculation and the paper.

- Dolan, J. F., S. A. Christofferson, and J. H. Shaw (2003), Recognition of paleoearthquakes on the Puente Hills blind thrust fault California, *Science*, *300*, 115–118.
- Field, E. H., et al. (2013), Uniform California earthquake rupture forecast, version 3 (UCERF3)—The time-independent model: U.S. Geological Survey Open-File Report 2013–1165, 97 p., California Geological Survey Special Report 228, and Southern California Earthquake Center Publication 1792. [Available at <http://pubs.usgs.gov/of/2013/1165/>.]
- Fielding, E. J., P. Milillo, R. Bürgmann, S.-H. Yun, Z. Liu, S. Samsonov, P. Agram, and G. Milillo (2015), California 2014 earthquake deformation imaged with InSAR time series: La Habra and South Napa, Fringe 2015 Workshop, Frascati (Rome), Italy.
- Hauksson, E., and S. Gross (1991), Source parameters of the 1933 Long Beach earthquake, *Bull. Seismol. Soc. Am.*, *81*(1), 81–98.
- Hauksson, E., and L. M. Jones (1991), The 1988 and 1990 upland earthquakes: Left-lateral faulting adjacent to the Central Transverse Ranges, *J. Geophys. Res.*, *96*(B5), 8143–8165, doi:10.1029/91JB00481.
- Holliday, J. R., K. Z. Nanjo, K. F. Tiampo, J. B. Rundle, and D. L. Turcotte (2005), Earthquake forecasting and its verification, *Nonlinear Processes Geophys.*, *12*, 965–977.
- Holliday, J. R., C. C. Chien, K. F. Tiampo, J. B. Rundle, D. L. Turcotte, and A. Donnellan (2007), A RELM earthquake forecast based on pattern informatics, *Seismol. Res. Lett.*, *78*(1), 87–93.
- Holliday, J. R., W. R. Graves, J. B. Rundle, and D. L. Turcotte (2014), Computing earthquake probabilities on global scale, *PAGEOPH*, doi:10.1007/s00024-014-0951-3.
- Kanamori, H. (1978), Quantification of earthquakes, *Nature*, *271*, 411–414.
- Kohler, M., H. Magistrale, and R. Clayton (2003), Mantle heterogeneities and the SCEC three-dimensional seismic velocity model version 3, *Bull. Seismol. Soc. Am.*, *93*, 757–774.
- Leon, L. A., S. A. Christofferson, J. F. Dolan, J. H. Shaw, and T. L. Pratt (2007), Earthquake-by-earthquake fold growth above the Puente Hills blind thrust fault, Los Angeles, California: Implications for fold kinematics and seismic hazard, *J. Geophys. Res.*, *112*, B03S03, doi:10.1029/2006JB004461.
- Mori, J., and R. E. Abercrombie (1997), Depth dependence of earthquake frequency-magnitude distributions in California: Implications for rupture initiation, *J. Geophys. Res.*, *103*, 15,081–15,090, doi:10.1029/97JB01356.
- Myers, D. J., J. L. Nabelek, and R. S. Yeats (2003), Dislocation modeling of blind thrusts in the eastern Los Angeles basin, California, *J. Geophys. Res.*, *108*(B9), 2443, doi:10.1029/2002JB002150.
- Pratt, T. L., J. H. Shaw, J. F. Dolan, S. A. Christofferson, R. A. Williams, and J. K. Odum (2002), Shallow seismic imaging of folds above the Puente Hills blind-thrust fault, Los Angeles, California, *Geophys. Res. Lett.*, *29*(9), 1304, doi:10.1029/2002JB002150.
- Roten, D., K. B. Olsen, S. M. Day, Y. Cui, and D. Fäh (2014), Expected seismic shaking in Los Angeles reduced by San Andreas fault zone plasticity, *Geophys. Res. Lett.*, *41*, 2769–2777, doi:10.1002/2014GL059411.
- Rundle, J. B., K. F. Tiampo, W. Klein, and J. S. S. Martins (2002), Self-organization in leaky threshold systems: The influence of near mean field dynamics and its implications for earthquakes, neurobiology and forecasting, *Proc. Natl. Acad. Sci. U.S.A.*, *99*(Suppl. 1), 2514–2521.
- Rundle, J. B., D. L. Turcotte, C. Sammis, W. Klein, and R. Shcherbakov (2003), Statistical physics approach to understanding the multiscale dynamics of earthquake fault systems (invited), *Rev. Geophys.*, *41*(4), 1019, doi:10.1029/2003RG000135.
- Rundle, J. B., J. R. Holliday, W. R. Graves, and D. L. Turcotte (2012), Tiampo, KF and W Klein, probabilities for large events in driven threshold systems, *Phys. Rev. E*, *86*, 021106.
- Rundle, J. B., et al. (2016), A practitioner's guide to earthquake forecasting, to appear, in *Applied Geology in California, Assoc. Environ. Eng. Geol. Spec. Publ.*, vol. 26, edited by R. Anderson and H. Ferriz, Star Publ. Co., Redwood City, Calif.
- Seeber, L., and J. G. Armbruster (1995), The San Andreas Fault system through the Transverse Ranges as illuminated by earthquakes, *J. Geophys. Res.*, *100*(B5), 8285–8310, doi:10.1029/94JB02939.
- Shaw, J. H., A. Plesch, J. F. Dolan, T. L. Pratt, and P. Fiore (2002), Puente Hills blind-thrust system, Los Angeles, California, *Bull. Seismol. Soc. Am.*, *92*(8), 2946–2960.
- Sleep, N. H. (2015), Long-term deformation driven by small ambient tectonic stresses and strong oscillating tidal within Enceladus with analogy to rock behavior near the San Andreas Fault, *Geochem. Geophys. Geosyst.*, *16*, 1670–1686, doi:10.1002/2015GC005725.
- Tiampo, K. F., J. B. Rundle, S. McGinnis, S. Gross, and W. Klein (2002), Mean field threshold systems and phase dynamics: An application to earthquake fault systems, *Europhys. Lett.*, *60*, 481–487.
- Tully, S., and L. Casiano Jr. (2014), Quake's effect on pipes, *Orange County Register*, July 31, 2014, pg A.
- Walls, C., T. Rockwell, K. Mueller, Y. Bock, S. Williams, J. Pfanner, J. Dolan, and P. Fang (1998), Escape tectonics in the Los Angeles metropolitan region and implications for seismic risk, *Nature*, *394*, 356–360.
- Weibull, W. (1951), A statistical distribution function of wide applicability, *J. Appl. Mech.*, *18*, 293–297.
- Wiskol, M. (2014), Quake's damage toll mounts, *Orange County Register*, April 8, 2014, Local p. 1.
- Wright, T. L. (1991), Structural geology and tectonic evolution of the Los Angeles Basin, in *Active Margin Basins*, edited by K. T. Biddle, *Mem. Am. Assoc. Pet. Geol.*, *52*, 35–134.
- Yang, W., and E. Hauksson (2011), Evidence for vertical partitioning of strike-slip and compressional tectonics from seismicity, focal mechanisms, and stress drops in the east Los Angeles basin area, California, *Bull. Seismol. Soc. Am.*, *101*(3), 964–974, doi:10.1785/0120100216.
- Yeats, R. S. (2004), Tectonics of the San Gabriel Basin and surroundings, Southern California, *Geol. Soc. Am. Bull.*, *116*(9–10), 1158–1182, doi:10.1130/B25346.1.

Erratum

In the originally published version of this article, some numerical expressions were incorrect. The numerical expressions have since been corrected, and this version may be considered the authoritative version of record.